Application of Simulated Countercurrent Moving-Bed Chromatographic Reactor for MTBE Synthesis

Ziyang Zhang, K. Hidajat, and Ajay K. Ray*

Department of Chemical and Environmental Engineering, The National University of Singapore, 10 Kent Ridge Crescent, Singapore 119260

Synthesis of MTBE directly from methanol and *tert*-butyl alcohol is considered in a separative chemical reactor, which can be used to simulate a countercurrent chromatographic moving bed. A mathematical model is developed for a reactor configuration consisting of multiple columns connected in series in a circular arrangement with ports that can serve either as inlets or as outlets. The columns are packed with Amberlyst 15 ion-exchange resin, which acts as both adsorbent and catalyst. Experimentally determined adsorption and kinetic parameters are used in the mathematical model to predict the concentration profiles of the reactant and products. The effects of the switching time; the feed, solvent, and product flow rates; and the number of columns on the yield, selectivity, and purity of the desired product (MTBE) and the conversion of the limiting reactant (TBA) were studied systematically. The sensitivity study reveals that it is not possible to maximize the yield and selectivity of MTBE simultaneously, as some of the operating parameter act in conflicting manners.

Introduction

Chromatographic separation is one of the most important separation methods and is widely used in industry because of its high separating power, selectivity, versatility, relatively low costs, and mild operating conditions, especially at analytical level. Chromatographic reactors are devices in which two different processes, namely, chemical reaction and separation of the reactants and products, take place concurrently. In recent years, researchers have focused on the development of simulated countercurrent moving-bed chromatographic reactor (SCMCR) systems, which preserve the inherent advantages of continuous countercurrent operation while at the same time helping to avoid the problems associated with the movement of solids that occurs in true countercurrent moving beds. Simulated moving-bed (SMB) technology, which maintains the separating power of moving beds, has been widely applied in recent years in the petrochemical, biochemical, and fine chemical industries.

In the simulated system, a fixed bed is used, and the countercurrent movement is simulated by successively switching the feed position through a series of inlets located at intervals along a single column[1] or between a series of packed columns[2] at timed intervals. In other words, the flow of solids past a fixed point is replaced by the motion of the feed past a fixed packed bed. Feed enters a particular column for a predetermined length of time and then is switched to the next column. Product streams are also advanced simultaneously. When the feed point has progressed to the end, it is returned to the starting position, and the process is repeated. The shifting of the feed and product positions in the direction of the fluid flow thus mimics the movement of solids in the opposite direction. The required motion between the feed and the bed, which is continuous for true countercurrency, is replaced by periodic discrete steps in simulated counter-currency. However, for all practical purposes, simulated countercurrent operation is continuous in that the rates and compositions of all streams entering and leaving the adsorbent bed are continuous functions without the associated problems of actual conveyance of solids. This eliminates the problems of solids handling, fines removal, solids recycling, and flow channeling. The required reactor volume is less as bed expansion, which is a problem in moving beds, does not occur in the simulated system. Moreover, in this system, because top and bottom reservoirs for feeding and collecting of solids are not necessary, required solids inventory is lower, thereby minimizing catalyst (and adsorbent) costs for the solid-catalyzed reactions.

In chromatographic reactors, because separation takes place at the site of chemical reaction, the rate of rthe everse reaction decreases, so that an equilibrium-limited reaction can be forced to near completion toward the formation of products beyond the amounts prescribed by thermodynamic equilibrium. Hence, SCMCR is a multifunctional reactor that simultaneously improves product purity and conversion by separating the product from the reactant (for example, $A \Leftrightarrow B$) or the desired product from a mixture of products (for example, $A + B \Leftrightarrow C + D + ...$) at the site of reaction. Therefore, equilibrium-limited reactions can be taken to significantly higher conversion than would be possible in reactors where separation does not take place. These reactors can have economic advantages over more conventional reactors, not only because conversion can be enhanced, but also because chromatographic separation does away with, or at least decreases, both the capital and energy costs of separating the reactants and products. This novel reactor helps in eliminating or greatly simplifying any subsequent separation operations that would be necessary if a nonseparative reactor were employed. The advantages of simulated countercurrent configuration are two-fold. The countercurrent movement of the fluid phase past the solid phase enables the system to be operated in continuous mode,

* Author to whom correspondence should be addressed. Fax: +65 779 1936. E-mail: cheakr@nus.edu.sg.

10.1021/ie001071+ CCC: $20.00
Published on Web 06/19/2001

thus improving the productivity. Simulating this movement, by switching feed points past fixed columns, helps to overcome the problems that arise as a result of solids flow. These features make SCMCRs attractive candidates for chemical processing.[1]

The interest in SCMCRs has been growing in the past 20 years, probably because of the success in SMB industrialization and their potential for use as integrated reactor−separators. Like reactive distillation, which couples distillation and chemical reaction together in one process, SCMCR technology combines the more powerful and energy-saving separation of SMB technology with a reversible chemical reaction in one reactor. The principle of successive switching and equipment of this type have been very successfully developed by UOP in their Sorbex process for liquid-phase separations. Various classes of important reactions, both chemical and biochemical, have been carried out in SCMCRs. Hashimoto et al.[3,4] studied the application of a continuous moving-column chromatographic separator to the enzymatic isomerization of glucose to fructose. They reported fructose purities of up to 65% using less desorbent than required for fixed-bed batch processes. However, their system does not fall exactly into the category of SCMCRs, as they used separate columns for reaction and separation. Ray et al.[1] applied SCMCR technology to a reversible gas-phase hydrogenation reaction of the type A ⇔ B for which the equilibrium conversion is 62%. They developed two different mathematical models of SCMCRs, an equilibrium-stage model[1] and a differential model,[2] for two different configurational approaches to the SCMCR. Model predictions of the concentration profiles in the reactor column (or columns) for the hydrogenation of mesitylene to trimethylcyclohexane at 463 K were reported. They demonstrated that reaction and separation can be achieved simultaneously and that the yield of the reaction can be greatly improved. Nearly unit conversion and 98−99% product purity were observed when appropriate operating conditions were used. Later, they verified their model predictions with an experimental investigation of the same reaction and observed very good agreement.[5] Tonkovich and Carr[6−8] reported experimental and modeling studies for the oxidative coupling of methane to form ethane and ethylene in a SCMCR. They used a four-section SCMCR that consisted of four fixed-bed reactor sections containing Sm_2O_3 catalyst maintained at 1000 K, followed by separative columns packed with activated charcoal adsorbent at 373 K. They obtained 65% methane conversion, 80% C_2 selectivity, and a C_2 yield of slightly better than 50% for the reaction, even though it is difficult to obtain a C_2 yield in excess of 20−25% by other methods. Kruglov[9] carried out a numerical modeling study on methanol synthesis for adiabatic or isothermal operation of SCMCR. They reported a CO conversion of as high as 96−99%. Kawase et al.[10] applied SCMCR technology to the organic synthesis of β-phenethyl acetate ester from acetic acid and β-phenethyl alcohol. They reported an esterification conversion of more than 99%, far beyond the equilibrium conversion of 63%. Mazzotti and co-workers[11] reported the synthesis of ethyl acetate ester using an ion-exchange resin (Amberlyst 15) in a laboratory unit of SCMCR.

Although a reasonable number of experimental and numerical studies on SCMCRs have been reported in the literature, there are still no reported applications of SCMCRs in the chemical industry. A more detailed understanding and criteria for operating SCMCRs are needed before successful applications can be achieved. The objective of this work is to determine the extent to which the moving-bed reactor's advantages of high purity and favorable equilibrium shifts are retained in SCMCRs for the direct synthesis of MTBE from TBA and methanol using Amberlyst 15 ion-exchange resin.

Direct Synthesis of MTBE

Methyl tertiary-butyl ether (MTBE) is currently the most important high-octane blending oxygenate for gasoline, which helps motor vehicles burn fuel more cleanly replacing toxic additives such as lead. The production and import of MTBE in the U.S. reached their highest levels in 1998,[12] although there is debate on the use of MTBE, especially in California. MTBE is commercially synthesized by the reversible etherification of isobutene with methanol using an acidic ion-exchange resin as a catalyst under a pressure high enough to maintain the reaction system in the liquid phase. However, a problem concerning MTBE production from isobutene is that the source of isobutene (IB) is limited to catalytic-cracking and steam-cracking fractions from petroleum refining. In this work, we report the direct synthesis of MTBE by reacting *tert*-butyl alcohol (TBA) with methanol. Amberlyst 15 ion-exchange resin is used, which acts as both catalyst and adsorbent for the etherification reaction in the SCMCR.

For the TBA−methanol−acid ion exchange system, the following three reactions can take place:

$$\mathrm{TBA} \rightleftharpoons \mathrm{IB} + \mathrm{H_2O} \quad (1)$$

$$\mathrm{IB} + \mathrm{MeOH} \rightleftharpoons \mathrm{MTBE} \quad (2)$$

$$\mathrm{TBA} + \mathrm{MeOH} \rightleftharpoons \mathrm{MTBE} + \mathrm{H_2O} \quad (3)$$

If IB produced in the first reaction is consumed instantaneously and completely according to the second reaction, then the overall reaction can be described by reaction 3. However, in our experimental studies, gas bubbles (isobutene) were detected in the effluent from a packed-bed reactor, as well as in experiments conducted in a well-stirred batch reactor using the same catalyst. Hence, the intermediate product, isobutene, is not consumed possibly because the rate of formation of IB in the first reaction is faster the rate of consumption in the second reaction. In this case, the third reaction takes place in addition to reactions 1 and 2. However, it can be noticed from the above three reactions that the overall amount of TBA consumed equals the overall amount of H_2O produced, and similarly for methanol consumed and MTBE produced. Consequently, the overall reaction can be described by the equation

$$n(\mathrm{CH_3})_3\mathrm{COH} + \mathrm{CH_3OH} \rightleftharpoons (\mathrm{CH_3})_3\mathrm{COCH_3} + n\mathrm{H_2O} + (n-1)(\mathrm{CH_3})_2\mathrm{CCH_2} \quad (4)$$

where n (usually greater than 1) is an unknown parameter, which indicates the ratio of reaction rates between the first (eq 1) and the second (eq 2) reactions and the amount of isobutene produced. However, if the isobutene produced is neglected, n is equal to 1, and eq 4 reduces to eq 3. It should also be noted that, although methanol is one of the reactants, it also acts as a carrier solvent and is usually present in excess. Its concentra-

tion varies very little during the entire reaction process and, therefore, can be regarded as constant. The concentration of isobutene on the solid phase can also be neglected as a result of its low boiling point, its being present in a trace amount, and most importantly, its very low affinity for the ion-exchange resin. A study on the reaction kinetics and adsorption isotherm for this reaction system has been reported elsewhere.[13]

Adsorbed TBA reacts with methanol to produce MTBE, H_2O, and IB as catalyzed by the dissociated protons present in the pores of the ion-exchange resin, which is initially saturated with methanol. The concentrations of MTBE and H_2O in the polymer phase depend on their adsorption equilibria, whereas the nonadsorbed isobutene desorbs into the liquid phase as soon as it is produced, so that it has no impact on the overall reaction rate. On the basis of these criteria, the following kinetic expression and the linear adsorption isotherm were proposed[13]

$$R = k_f\left[{q_{TBA}}^n - \frac{q_{MTBE}{q_{H_2O}}^n}{K_e}\right] \quad (5)$$

$$q_i = K_i C_i \quad (6)$$

where R is the reaction rate; q_i is the concentration of component i in the polymer phase; k_f is the forward reaction rate constant; K_e is the reaction equilibrium constant; and K_i and C_i are the adsorption constant and liquid-phase concentration, respectively, of component i.

Experiments were conducted at different temperatures, flow rates, and feed concentrations in a single packed column, and the elution (breakthrough) profiles of the various components from the exit of the column were monitored continuously. Two sets of experiments were performed. In the first set of experiments, binary mixtures of MTBE and H_2O in methanol were used as the feed to study their adsorption and desorption equilibria in the column. The second set of experiments was conducted to investigate the reaction kinetics. HPLC-grade methanol, MTBE, and TBA were used in all of the experimental runs. A HPLC column with a length of 0.25 m and an overall volume of 1.735×10^{-5} m^3 was used in the experimental study. It was packed with 9.66×10^{-3} kg of dry Amberlyst 15 resin. A water bath with a temperature controller was used to maintain constant temperature. A binary series 200 LC pump from Perkin-Elmer was connected to the packed bed to provide a rectangular pulse input of width t_p. Effluent from the exit of the column was collected manually at fixed time intervals (between 30 and 120 s, depending on flow rates used) interval. Analyses for methanol, TBA, and MTBE were carried out in a HP6890 gas chromatograph equipped with a 30-m-long OV-1 fused-silica capillary column from Ohio Valley. A volumetric Karl Fischer titrator with a model 100 titration controller from Denver Instrument was used to measure the concentration of water. Figure 1 shows the experimentally measured breakthrough curves of TBA, MTBE, and H_2O at three different temperatures. Experimental results show that H_2O travels more slowly than MTBE (less strongly adsorbed).

A mathematical model based on quasi-homogeneous kinetics was developed, which assumes the reaction in the polymer phase to be homogeneous.[13] The behavior

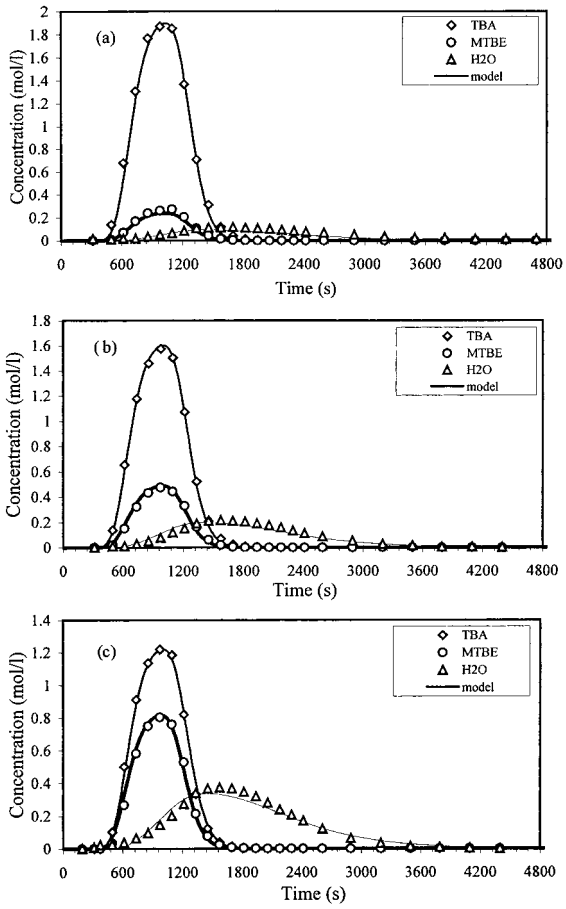

Figure 1. Effect of temperature on the breakthrough curves of TBA-H_2O-MTBE system. Experimental conditions: $Q = 1.67 \times 10^{-8}$ m^3/s, $t_p = 600$ s, $C_{TBA,f} = 2.189$ mol/L. (a) $T = 318$ K, (b) $T = 323$ K, (c) $T = 328$ K.

of reactants and products in a single fixed-bed reactor can be described by the mass balance equations for each component i (reactants and products) and can be written as

$$\frac{\partial C_i}{\partial t} + \left(\frac{1-\epsilon}{\epsilon}\right)\frac{\partial q_i}{\partial t} + \frac{u}{\epsilon}\frac{\partial C_i}{\partial z} - \left(\frac{1-\epsilon}{\epsilon}\right)\nu_i R = D_i\frac{\partial^2 C_i}{\partial z^2} \quad (7)$$

The initial and boundary conditions are given by

$$C_i(t=0) = C_i^{\,o} \quad (8)$$

$$C_i(0<t\le t_p)_{z=0} = C_{f,i} \quad (9)$$

$$C_i(t>t_p)_{z=0} = 0 \quad (10)$$

$$\left[\frac{\partial C_i(t)}{\partial z}\right]_{z=0} = 0 \quad (11)$$

where i = TBA, MTBE, and H_2O and u is the superficial fluid-phase velocity, which was assumed to be constant. The kinetic model assumes that the mobile and the stationary phases are always in equilibrium and that the contributions of all of the nonequilibrium effects can be lumped into an apparent axial dispersion coefficient, D. The PDE in eq 7, together with the initial and boundary conditions (eqs 8−11), the kinetic model equation (eq 5), and the adsorption equilibrium (eq 6) were solved using the method of lines.[14] In this tech-

Table 1. Adsorption Constants, K_i, Kinetic Parameters, k_f, K_e, and n, and Dispersion Coefficients, D_i

T (K)	K_{MTBE}	K_{H_2O}	K_{TBA}	k_f (mol$^{(1-n)}$ L$^{(n-1)}$/min)	K_e (mol/L)	n	10^6 D_{MTBE} (m^2/s)	10^6 D_{H_2O} (m^2/s)
318	0.375	2.846	0.460	0.025	24.682	1.018	1.948	7.092
323	0.330	2.800	0.440	0.060	20.943	1.092	2.333	7.708
328	0.300	2.750	0.460	0.112	18.202	1.120	2.350	8.167

nique, the PDE is first discretized in space using finite difference method (FDM) to convert it into a set of several-coupled ODE-IVPs. The resultant stiff ODEs of the initial value kind was solved using the subroutine, DIVPAG (which is based on Gear's method), in the IMSL library.

The kinetic parameters, adsorption equilibrium constants, and dispersion coefficients of TBA, MTBE, and H_2O in methanol were obtained by a least-squares fit that minimized the error between the experimental and model predicted results using the state-of-the-art genetic algorithm optimization method[15] and the values are given in Table 1 for three different temperatures. The concentration profiles given in Figure 1 show that the model (solid lines) can predict the experimental elution curves (symbols) quite well. The reliability and accuracy of the mathematical model were further verified when it was observed that the model could predict the experimental results fairly well at different feed concentrations and flow rates. The details are described in Zhang et al.[13]

Synthesis of MTBE in a SCMCR

Figure 2 shows a schematic diagram of a SCMCR and the principle of its operation. It consists of a number of columns of uniform cross section, each of length L and packed with the ion-exchange resin, which acts as both catalyst and adsorbent. The columns are connected in series in a circular array. Two incoming fluid streams (feed and eluent/desorbent) and two outgoing fluid streams (extract and raffinate) divide the reactor system into four sections (P, Q, R, and S), with p, q, r, and s representing the corresponding number of columns in each section, as illustrated in Figure 2. Q_p, the flow rate in section P, is regarded as the reference flow rate, on the basis of which all other flow rates are described. If α, β, and γ are assumed to be the ratios of the flow rates of feed (F), raffinate (Ra), and eluent (E), respectively, to the reference flow rate, Q_p, then the flow rates in each section can be defined as shown in Figure 2. Simulation of countercurrent movement of the solid is achieved by advancing the inlet and withdrawal ports, column by column, in the direction of the fluid flow at a predetermined switching time, t_s. However, to achieve separation between the components, the internal flow rates of the fluid phases within the four sections and the switching time (which defines the hypothetical solid-phase velocity) have to be specified appropriately. For a true countercurrent moving-bed chromatographic reactor (CMCR), Petroulas et al. (1985) defined the parameter σ_i, called the relative carrying capacity of the solid relative to the fluid stream for any component i, as

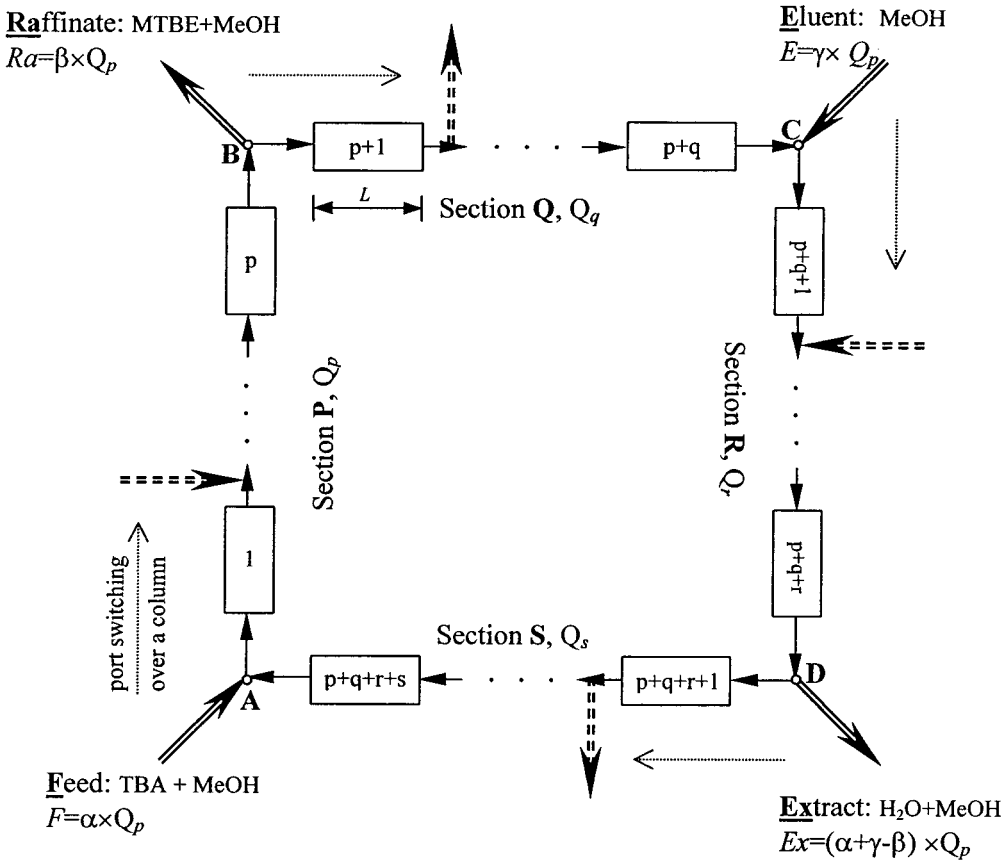

Figure 2. Schematic flow diagram of the SCMCR. The inlets and outlets divide the entire system into four sections, P, Q, R, and S with, respectively, p, q, r, and s columns. The flow rate in each section is given by $Q_q = (1 - \beta)Q_p$, $Q_r = (1 - \beta + \gamma)Q_p$, and $Q_s = (1 - \alpha)Q_p$.

$$\sigma_i = \frac{1-\epsilon}{\epsilon} NK_i \frac{u_s}{u_g} = \delta_i \frac{u_s}{u_g} \tag{12}$$

They showed that, to achieve countercurrent separation between two components, one must set σ greater than 1 for one component and less than 1 for the other. Later, Fish et al.[17] verified the above fact experimentally. Fish et al.[17] also defined V_i, the net velocity at which component i travels (or the concentration front moves) within the column, which, for a linear isotherm, is given by

$$V_i = \frac{u_g(1-\sigma_i)}{(1+\delta_i)} \tag{13}$$

Therefore, when $\sigma_i < 1$, $V_i > 0$ (species move with the fluid phase), and when $\sigma_i > 1$, $V_i < 0$ (species move with the solid phase). A fixed bed is represented by $\sigma = 0$. Ray et al.[1] redefined the above parameter, σ, for a SCMCR by replacing the solid-phase velocity, u_s, in a CMCR by a hypothetical solid-phase velocity, ζ, defined as $\zeta = L/t_s$ for SCMCR. They found, both theoretically[1] and experimentally,[5] that simulation of the countercurrent movement between two components can be achieved when redefined σ values were set such that σ is greater than 1 for one component and less than 1 for the other component. Hence, in the present study, if we set σ properly, the more strongly adsorbed component (H_2O) will move with the imaginary solid (resin) stream and can be collected at the extract port (point D in Figure 2), while at the same time, the less strongly adsorbed component (MTBE) will travel with the fluid stream and can be collected at the raffinate port (point B in Figure 2). It should also be noted that the parameter σ defined by the research group of Carr and Aris[16] is equivalent to β defined by the research group of Hashimoto,[3,4] γ defined by the research group of Ruthven,[18] and m defined by the research group of Morbidelli.[11]

Mathematical Model

The mathematical model for a SCMCR is similar to that established above for a single-column fixed-bed reactor, except that now there are multiple columns and switching is incorporated to mimic the movement of solids. The material balance given in eq 7 for a single column can be modified for a SCMCR system to

$$\frac{\partial C_{ij}^{(N)}}{\partial t} + \left(\frac{1-\epsilon}{\epsilon}\right)\frac{\partial q_{ij}^{(N)}}{\partial t} + \frac{u_\phi}{\epsilon}\frac{\partial C_{ij}^{(N)}}{\partial z} - \left(\frac{1-\epsilon}{\epsilon}\right)\nu_i R_j^{(N)} = D_i \frac{\partial^2 C_{ij}^{(N)}}{\partial z^2} \tag{14}$$

for component i in the jth column during the Nth switching period, where i = TBA, MTBE, or H_2O; u_ϕ designates the superficial flow rate in section ϕ (where ϕ = P, Q, R, or S); and the reaction rate and adsorption isotherm are given by and

$$R_j^{(N)} = k_f\left(q_{TBA,j}^{(N)\,n} - \frac{q_{MTBE,j}^{(N)}\, q_{H_2O,j}^{(N)\,n}}{K_e}\right) \tag{15}$$

$$q_{ij}^{(N)} = K_i C_{ij}^{(N)} \tag{16}$$

respectively. The initial and boundary conditions are given by

Initial conditions

$$\text{when } N = 0, \quad C_{ij}^{(0)} = C_{ij}^{\text{initial}} = 0 \tag{17}$$

when $N \geq 1$,

$$C_{ij}^{(N)} = C_{i,j+1}^{(N-1)} \quad \text{for} \quad j = 1 \text{ to } (N_{col}-1)$$

$$C_{ij}^{(N)} = C_{i1}^{(N-1)} \quad \text{for} \quad j = N_{col} \tag{18}$$

Boundary conditions

Feed point (point A)

$$C_{i1}^{(N)}|_{z=0} = (1-\alpha)C_{i,N_{col}}^{(N)}|_{z=L} + \alpha\, C_{i,f} \tag{19}$$

Raffinate withdrawal point (point B)

$$C_{i,p+1}^{(N)}|_{z=0} = C_{i,p}^{(N)}|_{z=L} \tag{20}$$

Eluent inlet point (point C)

$$C_{i,p+q+1}^{(N)}|_{z=0} = \left(\frac{1-\beta}{1-\beta+\gamma}\right)C_{i,p+q}^{(N)}|_{z=L} \tag{21}$$

Extract withdrawal point (point D)

$$C_{i,p+q+r+1}^{(N)}|_{z=0} = C_{i,p+q+r}^{(N)}|_{z=L} \tag{22}$$

The mass balance equation (eq 14), the initial (eqs 17 and 18) and boundary conditions (eqs 19−22), the kinetic equation (eq 15), and the adsorption isotherm (eq 16) completely define the SCMCR system. The PDEs were solved using the method of lines. The PDEs were first discretized in space using the finite difference method (FDM) to convert them into a set of several coupled ODE-IVPs, and the resultant stiff ODEs of the initial value kind were solved using the subroutine DIVPAG in the IMSL library. Because periodic switching is imposed on the system, the reactor works under transient conditions. Whenever switching is performed, a new initial value problem must be solved. However, a cyclic (periodic) steady state with a period equal to the switching time is eventually attained. After each switching, the column numbering was redefined according to eq 23 so that feed is always introduced into the first column.

before switching	after switching
column 1	column N_{col}
column j	column $j-1$, $j = 2, 3, \ldots, N_{col}$

(23)

The concentration profiles were obtained from the solution of the above equations (eqs 14−23). The objectives of this work are to determine whether we can achieve a higher conversion and improve the product purity for MTBE synthesis in a SCMCR. Therefore, the design of the SCMCR configuration and of the operating conditions to be used therein must be such that the conversion of the limiting reactant TBA (X_{TBA}) and the yield (Y_{MTBE}), purity (P_{MTBE}), and selectivity (S_{MTBE}) of the desired product (MTBE) are maximized at the raffinate port. The four quantities are defined as

$$X_{\mathrm{TBA}} = \frac{(\text{TBA fed} - \text{TBA collected at raffinate and extract})}{\text{TBA fed}}$$

$$= \frac{\alpha C_{\mathrm{TBA,f}} t_s - [\beta \int_0^{t_s} C^{(N)}_{\mathrm{TBA},p}|_{z=L}\, \mathrm{d}t + (\alpha + \beta - \gamma) \int_0^{t_s} C^{(N)}_{\mathrm{TBA},p+q+r}|_{z=L}\, \mathrm{d}t]}{\alpha C_{\mathrm{TBA,f}} t_s} \quad (24)$$

$$Y_{\mathrm{MTBE}} = \frac{\text{MTBE collected}}{\text{TBA fed}} = \frac{\beta[\int_0^{t_s} C^{(N)}_{\mathrm{MTBE},p}|_{z=L}\, \mathrm{d}t]}{\alpha C_{\mathrm{TBA,f}} t_s} \quad (25)$$

$$P_{\mathrm{MTBE}} = \frac{\text{MTBE collected}}{[\text{MTBE} + \mathrm{H_2O} + \text{TBA}]\ \text{collected}} = \frac{\int_0^{t_s} C^{(N)}_{\mathrm{MTBE},p}|_{z=L}\, \mathrm{d}t}{\int_0^{t_s} (C^{(N)}_{\mathrm{MTBE},p} + C^{(N)}_{\mathrm{H_2O},p} + C^{(N)}_{\mathrm{TBA},p})|_{z=L}\, \mathrm{d}t} \quad (26)$$

$$S_{\mathrm{MTBE}} = \frac{\text{MTBE collected}}{[\text{MTBE} + \mathrm{H_2O}]\ \text{collected}} = \frac{\int_0^{t_s} C^{(N)}_{\mathrm{MTBE},p}|_{z=L}\, \mathrm{d}t}{\int_0^{t_s} (C^{(N)}_{\mathrm{MTBE},p} + C^{(N)}_{\mathrm{H_2O},p})|_{z=L}\, \mathrm{d}t} \quad (27)$$

Results and Discussion

The concentration profiles for the reactant (TBA) and products (MTBE and H_2O) within the columns were obtained for a SCMCR configuration consisting of two columns (of length 0.25 m) in each section. Figure 3 shows the concentration profiles of TBA, MTBE, and H_2O after 10, 25, 50, and 100 switching periods for a switching time of 840 s. The *x* axis shows the position along the eight columns. In the figure, feed always enters at location A (see Figure 2), the raffinate port (point B) is located at the end of column 2, eluent enters at the end of column 4 (entry to column 5), and extract is withdrawn at the end of column 6. The outlet from column 8 is recycled back to the bottom of column 1 (point A) mixed with the makeup feed. The parameters used in solving the model equations (eqs 14−23) are shown in Figure 3. The flow rates in each section were set so that $\sigma_{\mathrm{MTBE}} < 1$ and $\sigma_{\mathrm{H_2O}} > 1$. Figure 3 reveals that the SCMCR configuration considered for the synthesis of MTBE attained pseudo-steady state after 100 switching periods as there is no difference in the concentration profiles between $N = 75$ and $N = 100$. It is also apparent from the figure that the separation of the concentration fronts of the two products, MTBE and H_2O, which were withdrawn continuously from the raffinate and extract ports, respectively, indeed takes place. Under the operating conditions used, conversion of TBA can reach 94.4%, while the yield, selectivity, and purity of MTBE at the raffinate port can reach 63.2, 75.2, and 72.5%, respectively. This is in contrast to the equilibrium conversion of 85.3% in a single-column fixed-bed reactor at the same operating temperature. Corresponding values of the yield, selectivity, and purity for MTBE at equilibrium are 76.1, 47.2, and 43.2%, respectively (see Table 2).

The separation of the two products, MTBE and H_2O, at the site of reaction accounts for the enhancement in the reactant (TBA) conversion and the increase in the yield of the desired product (MTBE). However, the selectivity and purity deteriorated because all of the process parameters (particularly the flow rate in section S) were not set properly. This resulted in a high H_2O concentration in section S, which not only increased the rate of reverse reaction but also allowed a large amount of H_2O to break through at the raffinate port. Therefore, the flow rate in section S must be set appropriately, so that the (purge) columns are adequately cleaned.

As shown in Figure 1, H_2O adsorbs more strongly on the ion-exchange resin than MTBE. Effective separation of the two components is accomplished by appropriately selecting the switching time (and, hence, the fluid-phase velocity) such that the more strongly adsorbed component travels with the solid phase while the component

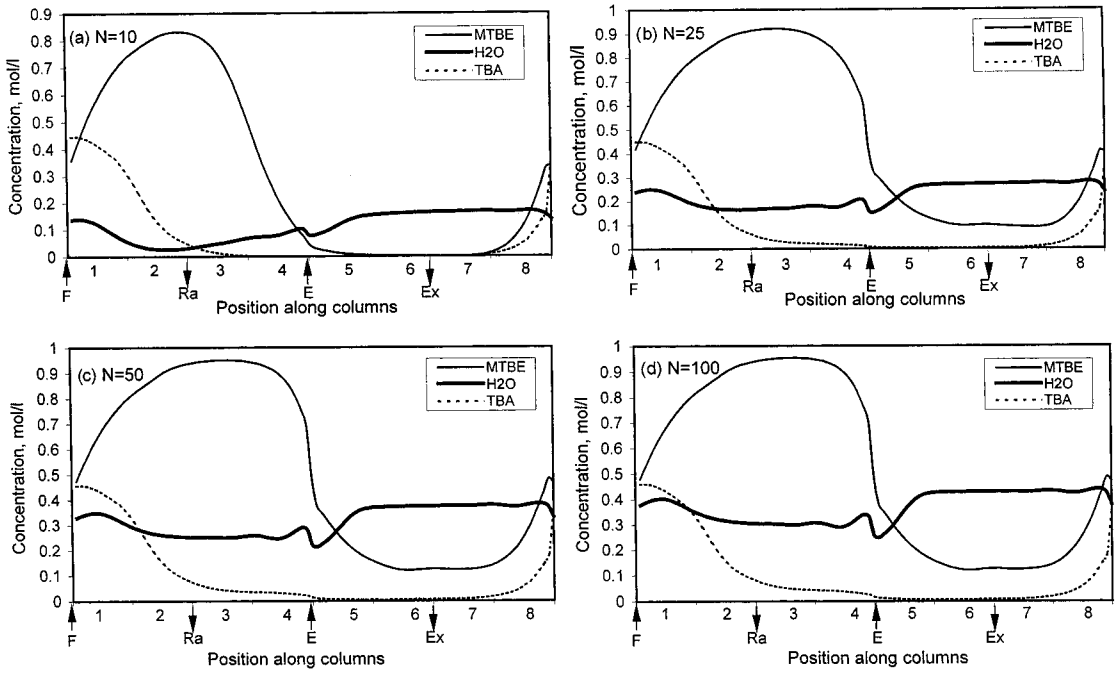

Figure 3. Concentration profiles of MTBE, H_2O and TBA. $T = 328$ K, $L = 0.25$ m, $t_s = 840$ s, $Q_p = 1.67 \times 10^{-8}$ m^3/s, $\alpha = \beta = 0.2$, $\gamma = 0.5$, $p = q = r = s = 2$, $\sigma_{\mathrm{MTBE,P}} = 0.223$, $\sigma_{\mathrm{H_2O,P}} = 2.046$. At $N = 100$, $X_{\mathrm{TBA}} = 94.4\%$, $S_{\mathrm{MTBE}} = 75.2\%$, $Y_{\mathrm{MTBE}} = 63.2\%$, $P_{\mathrm{MTBE}} = 72.5\%$.

Table 2. Effects of Switching Time, Solvent and Raffinate Flow Rates, and Number of Columns on Conversion of TBA and Yield, Purity, and Selectivity of MTBE

	$\sigma_{MTBE,P}$	$\sigma_{H_2O,P}$	X_{TBA} (%)	Y_{MTBE} (%)	P_{MTBE} (%)	S_{MTBE} (%)	figure
reference value[a]	0.223	2.046	94.4	63.2	72.5	75.2	3d
equilibrium (L = large)	0	0	85.3	76.1	43.2	47.2	–
effect of switching time, t_s							
$t_s = 600$ s	0.312	2.864	87.7	1.3	5.6	6.2	4a
$t_s = 1080$ s	0.174	1.591	91.8	44.7	65.8	71.7	4b
effect of solvent flow rate, γ							
$\gamma = 1$	0.223	2.046	96.9	63.1	86.6	89.2	5a
$\gamma = 2$	0.223	2.046	98.4	62.9	97.9	99.9	5b
effect of raffinate flow rate, β							
$\gamma = 2, \beta = 0.5$	0.223	2.046	97.6	87.4	96.4	98.7	6a
$\gamma = 2, \beta = 0.75$	0.223	2.046	97.1	87.3	90.6	93.1	6b
effect of number of columns							
$\gamma = 2, \beta = 0.5, p = 1, s = 3, t_s = 840$ s	0.223	2.046	85.2	76.8	82.3	97.8	7a
$\gamma = 2, \beta = 0.5, p = 1, s = 3, t_s = 720$ s	0.260	2.387	91.8	53.6	82.0	90.9	7b
$\gamma = 2, \beta = 0.5, p = 3, s = 1, t_s = 840$ s	0.223	2.046	92.4	77.6	98.2	98.7	8a
$\gamma = 2, \beta = 0.5, p = 3, s = 1, t_s = 960$ s	0.195	1.790	95.2	83.9	98.0	99.9	8b

[a] Reference: $T = 328$ K, $L = 0.25$ m, $Q_p = 1.67 \times 10^{-8}$ m^3/s, $t_s = 840$ s, $\alpha = 0.2$, $\beta = 0.2$, $\gamma = 0.5$, $p = q = r = s = 2$. Parameter values are the same as the reference values unless mentioned otherwise.

with the weaker affinity travels with the fluid phase. There is, however, a complex interplay of the various operating parameters of the SCMCR, namely, switching time (t_s), fluid flow rate in each section j (Q_j), fractions of feed (α) and eluent (γ) inflow and raffinate (β) collected, temperature (T), feed concentration of TBA ($C_{TBA,f}$), and number of columns (p, q, r, and s) in sections P, Q, R, and S (see Figure 2). All of these operating parameters influence the value of the solid-phase pseudo-velocity (ζ) and the σ_i (eq 12) and V_i (eq 13) values for each component i in each section j, which eventually alters the values of X_{TBA}, Y_{MTBE}, S_{MTBE}, and P_{MTBE}.

Effect of Switching Time, t_s. The effect of the switching time, t_s, is illustrated in Figure 4, where concentration profiles of TBA, MTBE, and H_2O are shown for the switching times of 600 and 1080 s compared to t_s of 840 s (Figure 3). All other parameters were kept constant as in Figure 3. When the switching time was reduced to 600 from 840 s, the conversion of TBA obtained was 87.7% (slightly lower), while the yield, selectivity, and purity of MTBE at the raffinate port obtained were 1.3, 6.2, and 5.6%, respectively, which were significantly lower than the values obtained when the switching time was 840 s. The reduction of the switching time increased the solid-phase pseudo-velocity, ζ (4.167×10^{-4} m/s compared to 2.976×10^{-4} m/s when $t_s = 840$ s) while decreasing the residence time of reactant in each section, thereby lowering the conversion of TBA. The increase of ζ also altered the σ values of the two products in section P. The values of σ_{MTBE} and σ_{H_2O} changed to 0.312 and 2.864 compared to 0.223 and 2.046, respectively, while the velocities with which the two components traveled in the fluid and solid phases, V_{MTBE} and V_{H_2O}, changed to 2.84×10^{-4} and -2.18×10^{-4} m/s from 3.22×10^{-4} and -1.22×10^{-4} m/s, respectively. This effectively increased the net separation of the concentration fronts of the two products, MTBE and H_2O (ΔV increased from 4.44×10^{-4} to 5.22×10^{-4} m/s), thereby enhancing the separation (by 13.6%) between the two components. Consequently, this is expected to increase the selectivity and purity of MTBE at the raffinate port. However, we observe a drastic deterioration of these two values, which can be easily understood by examining the values of σ and V for the two components in section Q. The strongly adsorbed component (H_2O) travels at a much faster rate with the solid phase when t_s is lowered and eventually appears in the product stream at the raffinate port, thereby lowering the selectivity and purity of MTBE. This also reduces the yield of MTBE at the raffinate port considerably as a result of the reduction in the conversion of TBA (because of the lower residence time) and the increase in the reverse reaction rate because of the increase in the H_2O concentration. Because all components travel relatively more with the solid phase, the weakly adsorbed product MTBE accumulate mostly behind the feed point, i.e., in section S instead of at the raffinate port.

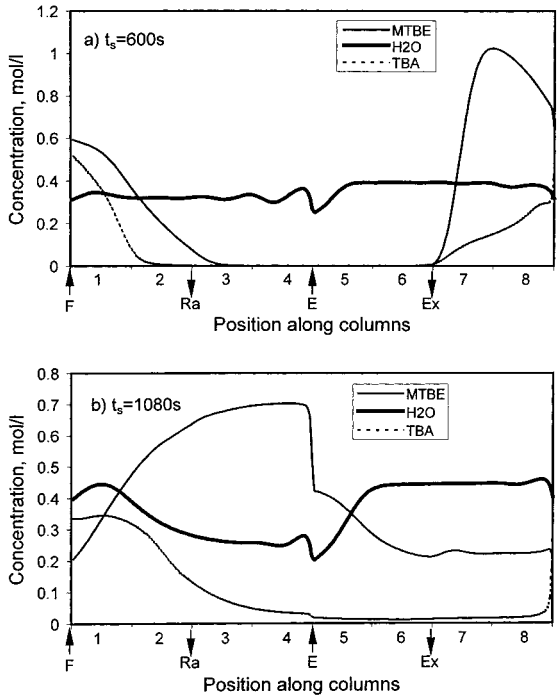

Figure 4. Effect of switching time on steady-state concentration profiles of MTBE, H_2O, and TBA after 100 switching periods. $T = 328$ K, $Q_p = 1.67 \times 10^{-8}$ m^3/s, $\alpha = \beta = 0.2$, $\gamma = 0.5$, $p = q = r = s = 2$, (a) $\sigma_{MTBE,P} = 0.312$, $\sigma_{H_2O,P} = 2.864$, $X_{TBA} = 87.7\%$, $S_{MTBE} = 6.2\%$, $Y_{MTBE} = 1.3\%$, $P_{MTBE} = 5.6\%$. (b) $\sigma_{MTBE,P} = 0.174$, $\sigma_{H_2O,P} = 1.591$, $X_{TBA} = 91.8\%$, $S_{MTBE} = 71.7\%$, $Y_{MTBE} = 44.7\%$, $P_{MTBE} = 65.8\%$.

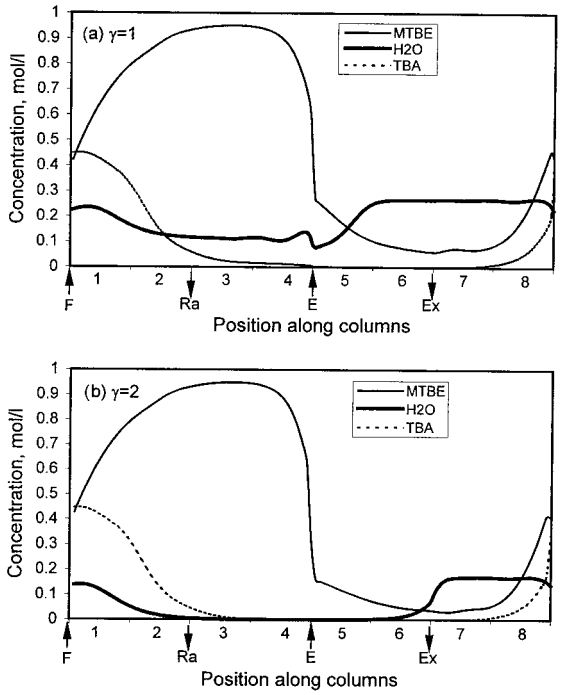

Figure 5. Effect of solvent flow rate on steady-state concentration profiles of MTBE, H_2O, and TBA after 100 switching periods. T = 328 K, t_s = 840 s, $Q_p = 1.67 \times 10^{-8}$ m^3/s, $\alpha = \beta = 0.2$, $p = q = r = s = 2$. (a) $\sigma_{MTBE,P} = 0.223$, $\sigma_{H_2O,P} = 2.046$, $X_{TBA} = 96.9\%$, $S_{MTBE} = 89.2\%$, $Y_{MTBE} = 63.1\%$, $P_{MTBE} = 86.6\%$. (b) $\sigma_{MTBE,P} = 0.223$, $\sigma_{H_2O,P} = 2.046$, $X_{TBA} = 98.4\%$, $S_{MTBE} = 99.9\%$, $Y_{MTBE} = 62.9\%$, $P_{MTBE} = 97.9\%$.

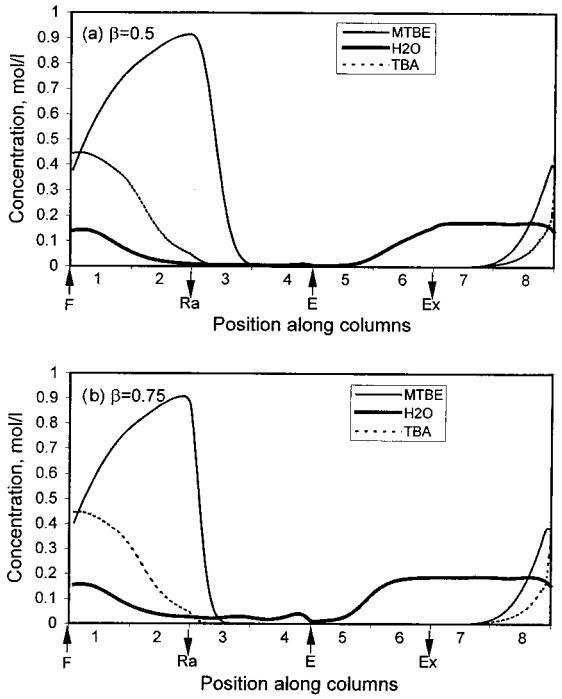

Figure 6. Effect of raffinate flow rate on steady-state concentration profiles of MTBE, H_2O, and TBA after 100 switching periods. T = 328 K, t_s = 840 s, $Q_p = 1.67 \times 10^{-8}$ m^3/s, $\alpha = 0.2$, $\gamma = 2$, $p = q = r = s = 2$. (a) $\sigma_{MTBE,P} = 0.223$, $\sigma_{H_2O,P} = 2.046$, $X_{TBA} = 97.6\%$, $S_{MTBE} = 98.7\%$, $Y_{MTBE} = 87.4\%$, $P_{MTBE} = 96.4\%$. (b) $\sigma_{MTBE,P} = 0.223$, $\sigma_{H_2O,P} = 2.046$, $X_{TBA} = 97.1\%$, $S_{MTBE} = 93.1\%$, $Y_{MTBE} = 87.3\%$, $P_{MTBE} = 90.6\%$.

In contrast, when switching time was increased to 1080 s, the solid-phase pseudo-flow rate was reduced, and therefore, most of the components traveled more with the fluid phase than with the solid phase. As illustrated in Figure 4b, although more H_2O and MTBE appeared in section P, a large concentration of MTBE also emerged at the extract port. Consequently, MTBE and H_2O were not effectively separated. In this case, the conversion of TBA and the yield, selectivity, and purity of MTBE obtained were 91.8, 44.7, 71.7, and 65.8%, respectively.

Effect of Solvent Flow Rate, γ. In Figure 3d, we saw that, even though the conversion of TBA could reach 94.4% with a switching time of 840 s, an appreciable amount of H_2O was present at the raffinate port ($P_{MTBE} = 72.5\%$), presumably because H_2O was not effectively desorbed in sections R and S. Figure 1 reveals that, in addition to the strong affinity of H_2O for the resin (see Table 1), there is also a considerable tailing of the H_2O concentration front. Hence, with a faster switching speed, there is not enough time for H_2O to be completely desorbed from the purge column as the back of the H_2O concentration front spreads out (tails). Hence, this section will not be completely clean when a column in this segment subsequently becomes the feed column. Moreover, with a switching speed that is too large or too small, either H_2O shows up in the raffinate port, or MTBE shows up in the extract port. The only way to further promote separation at the reaction site is to completely wash out H_2O in the purge section by increasing the solvent flow rate.

Figure 5 illustrates the effect of the solvent (eluent or desorbent) flow rate (parameter γ) on the concentration profiles of the three components at pseudo-steady state (N = 100). All other parameters were kept the same as in Figure 3d. When γ was increased to 1.0 (compared to 0.5 in Figure 3d), less H_2O appeared at the raffinate port, as expected from Figure 5a. X_{TBA}, S_{MTBE}, and P_{MTBE} increased to 96.9, 89.2, and 86.6%, respectively, although Y_{MTBE} remained at almost the same value. When γ was increased further to 2.0 (Figure 5b), hardly any H_2O was present at the raffinate port, and nearly complete separation of the MTBE and H_2O concentration fronts could be achieved. Section R was essentially completely regenerated, and when a column in this section became the feed column, it was completely clean. The selectivity and purity of MTBE at the raffinate port reached 99.9 and 97.9%, respectively, while the conversion increased to 98.4%. However, the yield of MTBE still remained at a low value of 62.9%. Therefore, increasing solvent flow rate can enhance the selectivity, but not necessarily the yield, of the desired compound.

Effect of Raffinate Flow Rate, β. In the previous section, we observed that, by adjusting the solvent flow rate, the conversion and selectivity can be increased, but little effect on the yield can be achieved. In this section, we explore the effect of β on the yield and selectivity of MTBE, for which the results are shown in Figure 6. All parameters were kept constant at their reference values, including the switching time of 840 s, but γ was changed to 2.0 to determine whether β had any effect on the high value of the MTBE selectivity obtained for the conditions corresponding to Figure 5b. When β was increased to 0.5 (from 0.2), which indicates that half of the fluid stream was withdrawn at the raffinate port as product, Y_{MTBE} increased by 39% to 87.4% (Figure 6a), whereas X_{TBA} and S_{MTBE} remained almost at the same values. This is due to the increased separation between MTBE and H_2O obtained (which is reflected in the values of σ) as a result of the reduction of the fluid-phase velocity in sections Q and R. When

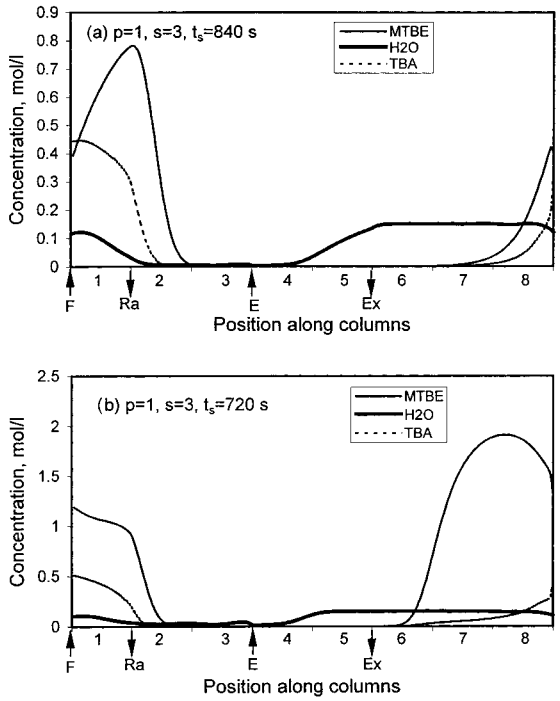

Figure 7. Effect of fewer columns in section P. $T = 328$ K, $Q_p = 1.67 \times 10^{-8}$ m^3/s, $\alpha = 0.2$, $\beta = 0.5$, $\gamma = 2$, $q = r = 2$. (a) $\sigma_{MTBE,P} = 0.223$, $\sigma_{H_2O,P} = 2.046$, $X_{TBA} = 85.2\%$, $S_{MTBE} = 97.8\%$, $Y_{MTBE} = 76.8\%$, $P_{MTBE} = 82.3\%$. (b) $\sigma_{MTBE,P} = 0.260$, $\sigma_{H_2O,P} = 2.387$, $X_{TBA} = 91.8\%$, $S_{MTBE} = 90.9\%$, $Y_{MTBE} = 53.6\%$, $P_{MTBE} = 82.0\%$.

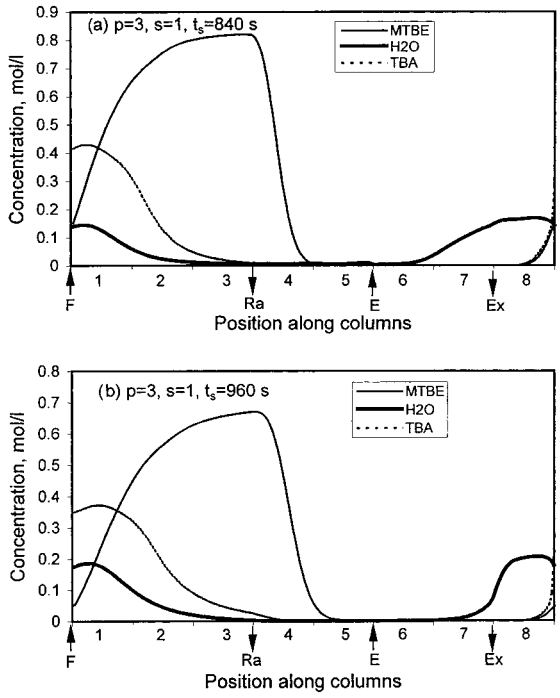

Figure 8. Effect of fewer columns in section S. $T = 328$ K, $Q_p = 1.67 \times 10^{-8}$ m^3/s, $\alpha = 0.2$, $\beta = 0.5$, $\gamma = 2$, $q = r = 2$. (a) $\sigma_{MTBE,P} = 0.223$, $\sigma_{H_2O,P} = 2.046$, $X_{TBA} = 92.4\%$, $S_{MTBE} = 98.7\%$, $Y_{MTBE} = 77.6\%$, $P_{MTBE} = 98.2.\%$. (b) $\sigma_{MTBE,P} = 0.195$, $\sigma_{H_2O,P} = 1.790$, $X_{TBA} = 95.2\%$, $S_{MTBE} = 99.9\%$, $Y_{MTBE} = 83.9\%$, $P_{MTBE} = 98.0\%$.

the β value was further increased to 0.75 (Figure 6b), the values of X_{TBA} and Y_{MTBE} remained almost unchanged (compared to $\beta = 0.5$), but S_{MTBE} decreased by 5.6% to 93.1% due to solvent flow that was insufficient to desorb H_2O completely in section Q.

Effect of Number of Columns in Sections P and S. The effects of the distribution of the number of columns in sections P and S were investigated next, while the numbers of columns in sections Q and R (the effects of which are shown later in Table 3) and the total number of columns, N_{col}, were fixed as before at 2, 2, and 8, respectively. Figure 7a shows the effect of reducing the number of columns in section P ($p = 1$, $s = 3$ instead of $p = 2$, $s = 2$) on the concentration profiles at $N = 100$ when all other parameter values are kept constant at the values given in Figure 6a. Compared to the results shown in Figure 6a, X_{TBA}, Y_{MTBE}, S_{MTBE}, and P_{MTBE} all decreased (see Table 2) when section P was reduced to a single column. Reducing number of columns in section P reduces the residence time of the reactant in this section, thereby reducing the conversion. The purity of MTBE decreased by a large amount as more TBA appeared at the raffinate port because of the reduced conversion. However, the selectivity of MTBE was barely affected as hardly any H_2O broke through at this port.

Reducing the switching speed for this new reactor configuration led to interesting behavior. When the switching speed was reduced to 720 s (from 840 s), the residence time in section P was reduced even further. Therefore, it is expected that the conversion would decrease. However, the opposite was observed. This can be understood if we scrutinize Figure 7b carefully. As TBA moves more slowly than MTBE ($K_{TBA} = 0.46$ and $K_{MTBE} = 0.3$ at $T = 328$ K), less TBA is collected at the raffinate port when t_s is reduced. Moreover, less TBA is also collected at the extract port, and therefore, conversion, as defined in eq 24, increases. The large increase in MTBE concentration in section S can be understood if we examine the velocities with which the concentration fronts move in this section. When t_s is reduced, the solid-phase pseudo-velocity is increased. The net velocities with which two concentration fronts move in section S for the conditions of Figure 7b are $V_{MTBE} = 2.23 \times 10^{-4}$ m/s and $V_{H_2O} = -1.86 \times 10^{-4}$ m/s, with a net separation of $\Delta V = 4.09 \times 10^{-4}$ m/s. This is in contrast to the values of $V_{MTBE} = 2.39 \times 10^{-4}$ m/s and $V_{H_2O} = -1.46 \times 10^{-4}$ m/s, with a net separation of $\Delta V = 3.85 \times 10^{-4}$ m/s, for the conditions of Figure 7a. With an increase in net separation between MTBE and H_2O in section S, forward reaction is favored, which increases the production of MTBE. As the residence time is increased with more columns ($s = 3$) in this section, more and more MTBE is formed. The yield and selectivity of MTBE at the raffinate port decrease because, with the increase in the recycling of MTBE to the feed column, the reverse reaction is favored, resulting inthe reduced collection of MTBE at point B. All of these counteracting effects result in an increase of X_{TBA}, but decreases Y_{MTBE} and S_{MTBE}.

Figure 8a shows the simulation results when the number of columns in section P was increased to 3 the number of columns in section S was simultaneously reduced to 1 to keep the total number of columns same (i.e., $p = 3$, $s = 1$, $N_{col} = 8$). Table 2 and Figure 8a reveal that X_{TBA} and Y_{MTBE} decreased but that P_{MTBE} increased compared to the values for the reference run of Figure 6a. This is contrary to what is expected, as with the increase in columns in section P, the residence time of the reactant increases in that segment, which should result in a high conversion of TBA. However, a close look at Figure 8a reveals that, with fewer columns in the purge section ($s = 1$), the column in section S is not clean initially when it becomes the feed column. Hence,

Table 3

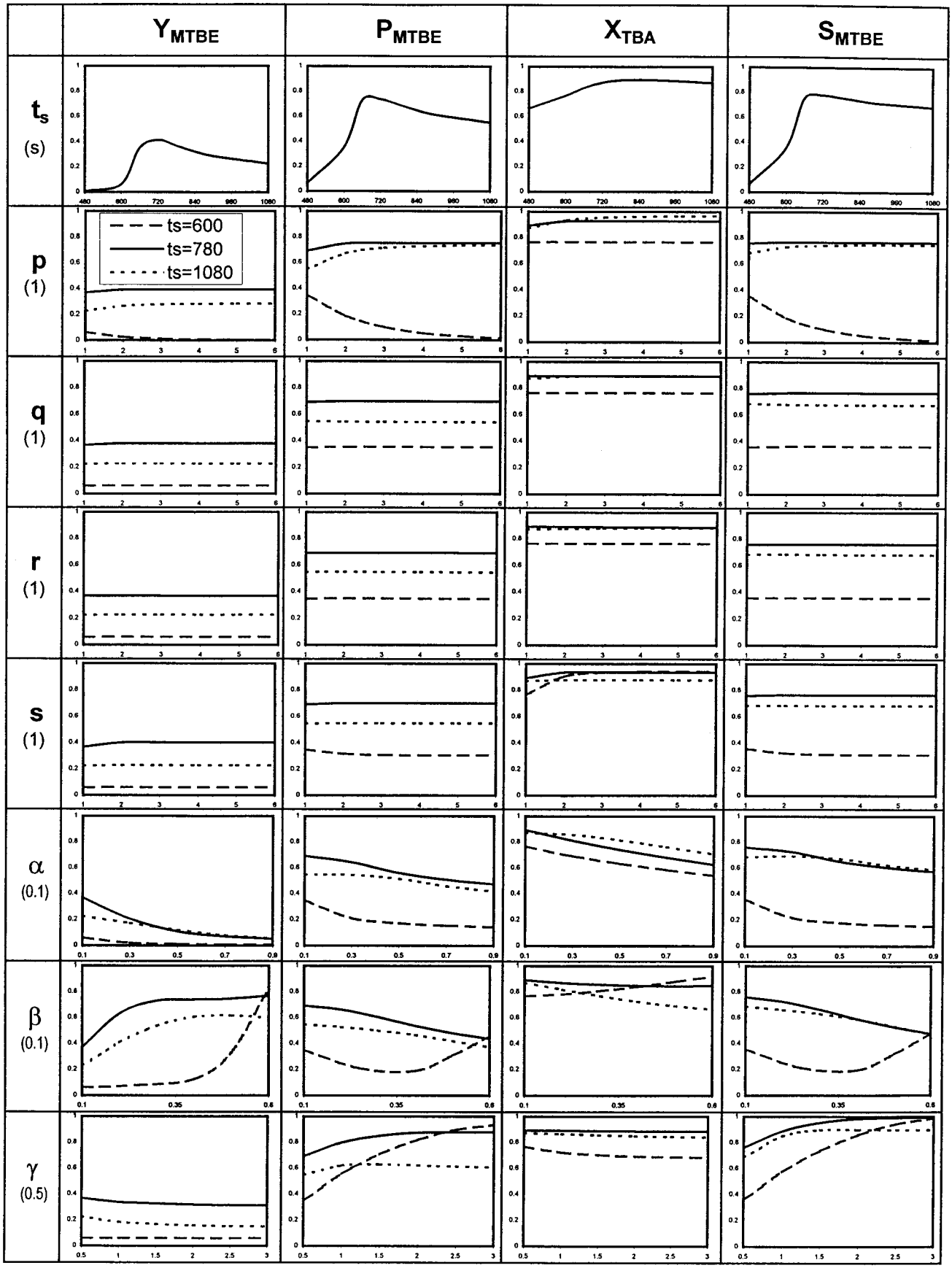

the conversion of TBA and the yield of MTBE decrease because of the increase in the extent of the reverse reaction, whereas the purity of MTBE at the raffinate port increases because of the increase in the residence time for the separation of the products. X_{TBA}, Y_{MTBE}, and S_{MTBE} can be increased even further if the switching period is increased (for example, to 960 from 840 s), which allows the columns of section S more time to

become clean. This is shown in Figure 8b. With increased residence times in sections P and S, there is more time for products to be separated, which ultimately increases X_{TBA}, Y_{MTBE}, and S_{MTBE}.

The effects of the parameters (t_s, β, γ, p, s, etc.) reveal that there is a complex interplay of all of these parameters on X_{TBA}, Y_{MTBE}, S_{MTBE}, and P_{MTBE}. If we want to maximize one (for example, Y_{MTBE}), another one (for example, P_{MTBE}) worsens. The optimum SCMCR configuration (number and length of columns) and operating conditions (such as t_s, β, γ, etc.) differ depending on which variable we want to maximize among X_{TBA}, Y_{MTBE}, S_{MTBE} and P_{MTBE}, and it might not be possible to maximize all at the same time. One might also find infinite optimal solutions, or a Pareto optimal solution, when one performs a multiobjective optimization of a SCMCR. A Pareto optimal solution is usually obtained when one or more of the decision variables are conflicting in nature. In Table 3, we show a sensitivity study of these parameters on the several objectives at 328 K when the carrier flow rate is $Q_p = 1.67 \times 10^{-8}$ m^3/s. The parameters on the left column of Table 3 denote the x-axis variable for the respective rows, while the number in parentheses denote the reference values of those parameters used in simulation runs for the other rows. The effects of each parameter on Y_{MTBE}, P_{MTBE}, X_{TBA}, and S_{MTBE} are shown for the reference values of the other parameters in the four subsequent columns. The effects of the switching time, t_s, are shown in the diagrams in the first row. Subsequently, three values of t_s (600, 780, and 1080 s) were used to show the influence of a particular parameter on Y_{MTBE}, P_{MTBE}, X_{TBA}, and S_{MTBE}.

Table 3 shows that q and r, which represent numbers of columns in sections Q and R, respectively, have no impact on the final results, when each of them is varied from 1 to 6. Some parameters, such as β and γ, have conflicting influences on the yield, purity, and selectivity of MTBE and on the conversion of TBA. Furthermore, depending on t_s, the effects of α, β, γ, and p are quite different. The influence of t_s is particularly complex. Its optimum value depends not only on the distribution of columns in different sections, but also on the values of α, β, and γ. One must perform multiobjective optimization to determine the optimal conditions and configuration of SCMCR along the same lines as recently reviewed by Bhaskar et al.[19]

Conclusions

In this work, the synthesis of MTBE by direct reaction between methanol and TBA on the acid ion-exchange resin Amberlyst 15 was considered in a simulated countercurrent moving-bed chromatographic reactor (SCMCR). The reactor consisted of series of columns connected in series in a circular array with a port between each column. Countercurrent motion was mimicked by continuously switching the reactant and product ports to simulate solid movement in the direction opposite to that of the fluid phase. A mathematical model was developed and solved using experimentally determined adsorption and kinetic parameters for the etherification reaction. The mathematical model can predict the concentration profiles of the reactant, TBA, and the products, MTBE and H_2O. The effects of the feed, solvent, and product flow rates, the switching time, and the number of columns in the SCMCR configuration on the concentration profiles of the three components; on the yield, selectivity, and purity of MTBE at the raffinate port; and on the conversion of the limiting reactant, TBA, were studied. It was observed that MTBE travels faster than H_2O, separation at the reaction site makes it possible to increase the yield and selectivity of MTBE, and the SCMCR configuration reaches a pseudo-steady state after 100 switching operations. The switching time and solvent flow rate play very important roles in achieving effective separation of the components. It was found that some of the process parameters not only alter the yield, selectivity, and purity of MTBE profoundly, but also act in conflicting manners. It is not possible to maximize the yield and selectivity simultaneously. By adjusting the process parameters, it is possible to reach conversions of TBA and selectivities and purities of MTBE as high as 98%, as well as yields of MTBE as high as 95%, although not all simultaneously. This is in contrast to the equilibrium conversion, yield, selectivity, and purity of 85.3, 76.1, 47.2, and 43.2%, respectively. The present study was conducted to study the effective design of a SCMCR without actually optimizing the entire process using multiobjective optimization techniques. Further improvement is expected if a systematic process optimization is conducted using multiple objectives.

Notation

C = liquid-phase concentration, mol/L
D = apparent axial dispersion coefficient, m^2/s
k = reaction rate constant
K = equilibrium constant
L = length of column, m
n = moles of TBA reacted per mole of methanol
N = number of switchings
p = number of columns in section P
P = purity
q = concentration in the polymer phase, mol/L; number of columns in section Q
Q = volume flow rate, m^3/s
r = number of columns in section R
R = reaction rate, mol/(min L)
s = number of columns in section S
S = selectivity
t = time, s
T = temperature, K
u = superficial velocity, m/s
V = velocity, m/s
X = conversion
Y = yield
z = axial coordinate, m

Greek Letters

α = fraction of feed
β = fraction of raffinate withdrawn
γ = fraction of eluent
δ = phase ratio
ϵ = void fraction
ϕ = section
σ = relative carrying capacity
ζ = solid-phase pseudo-velocity
ν = stoichiometric coefficient of component

Subscripts/Superscripts

o = initial, inlet
b = backward
col = column
e = equilibrium
f = feed, forward
g = gas, carrier

i = component i
j = column number
s = solid, switching
n = exponent
N = number, switching period
p = width of rectangular pulse

Literature Cited

(1) Ray, A. K.; Carr, R. W.; Aris, R. The simulated countercurrent moving-bed chromatographic reactor—A novel reactor separator. *Chem. Eng. Sci.* **1994**, *49* (4), 469−480.

(2) Ray, A. K.; Carr, R. W. Numerical simulation of a simulated countercurrent moving bed chromatographic reactor. *Chem. Eng. Sci.* **1995**, *50* (19), 3033−3041.

(3) Hashimoto, K.; Adachi, S.; Noujima, H.; Ueda, Y. A new process combining adsorption and enzyme reaction for producing higher fructose syrup. *Biotechnol. Bioeng.* **1983**, *25*, 2371−2393.

(4) Hashimoto, K.; Adachi, S.; Noujima, H.; Maruyama, A. Models for separation of a glucose−fructose mixture using a simulated moving bed adsorber. *J. Chem. Eng. Jpn.* **1983**, *16*, 400−406.

(5) Ray, A. K.; Carr, R. W. Experimental study of a laboratory-scale simulated countercurrent moving bed chromatographic reactor. *Chem. Eng. Sci.* **1995**, *50* (14), 2195−2202.

(6) Tonkovich, A. L.; Carr, R. W.; Aris, R. Enhanced C_2 yields from methane oxidative coupling by means of a separative chemical reactor. *Science* **1993**, *262*, 221−223.

(7) Tonkovich, A. L.; Carr, R. W. A simulated countercurrent moving-bed chromatographic reactor for the oxidative coupling of methane: Experimental results. *Chem. Eng. Sci.* **1994**, *49* (24a), 4647−4656.

(8) Tonkovich, A. L.; Carr, R. W. Modeling of the simulated countercurrent moving-bed chromatographic reactor used for the oxidative coupling of methane. *Chem. Eng. Sci.* **1994**, *49* (24a), 4657−4665.

(9) Kruglov, A. Methanol synthesis in a simulated countercurrent moving-bed adsorptive catalytic reactor. *Chem. Eng. Sci.* **1994**, *49* (24a), 4699−4716.

(10) Kawase, M.; Suzuki, T. B.; Inoue, K.; Yoshimoto, K.; Hashimoto, K. Increased esterification conversion by application of the simulated moving-bed reactor. *Chem. Eng. Sci.* **1996**, *51* (11), 2971−2976.

(11) Mazzotti, M.; Kruglov, A.; Neri, B.; Gelosa, D.; Morbidelli, M. A continuous chromatographic reactor: SMBR. *Chem. Eng. Sci.* **1996**, *51* (10), 1827−1836.

(12) Swain, E. J. U.S. MTBE production at a record high in 1998. *Oil Gas J.* **1999**, *97* (24), 99−101.

(13) Zhang, Z.; Hidajat, K.; Ray, A. K. Determination of Adsorption and Kinetic Parameters for Methyl *tert*-Butyl Ether Synthesis from *tert*-Butyl Alcohol and Methanol. *J. Catal.* **2001**, *200* (2), 209−221.

(14) Schiesser, W. E. *The Numerical Method of Lines: Integration of Partial Differential Equation: ODEs, DAEs, and PDEs*; Academic Press: New York, 1991.

(15) Goldberg, D. E. *Genetic Algorithms in Search, Optimization and Machine Learning*; Addison-Wesley: Reading, MA, 1989.

(16) Petroulas, T.; Aris, R.; Carr, R. W. Analysis and performance of a countercurrent moving-bed chromatographic reactor. *Chem. Eng. Sci.* **1985**, *40*, 2233−2240.

(17) Fish, B.; Carr, R. W.; Aris, R. The continuous countercurrent moving bed chromatographic reactor. *Chem. Eng. Sci.* **1986**, *41* (4), 661−668.

(18) Ruthven, D. M. The axial dispersed plug flow model for continuous counter-current adsorbers. *Can. J. chem. Eng.* **1983**, *61*, 881−883.

(19) Bhaskar, V.; Gupta, S. K.; Ray, A. K. Applications of multiobjective optimization in chemical engineering. *Rev. Chem. Eng.* **2000**, *16* (1), 1−54.

Received for review December 11, 2000
Revised manuscript received April 23, 2001
Accepted May 9, 2001

IE001071+